AGU PUBLICATIONS

Geophysical Research Letters

RESEARCH LETTER
10.1002/2016GL068497

All authors contributed equally.

Key Points:
- Underground nuclear tests by the DPRK have generated observable atmospheric infrasound
- During the 2013 and 2016 tests, the stratospheric waveguide was in a very different state
- We hypothesize that the 2016 test took place at least 1.5 times deeper than the 2013 test

Supporting Information:
- Supporting Information S1

Correspondence to:
J. D. Assink,
assink@knmi.nl

Citation:
Assink, J. D., G. Averbuch, P. S. M. Smets, and L. G. Evers (2016), On the infrasound detected from the 2013 and 2016 DPRK's underground nuclear tests, *Geophys. Res. Lett.*, *43*, 3526–3533, doi:10.1002/2016GL068497.

Received 2 MAR 2016
Accepted 18 MAR 2016
Accepted article online 22 MAR 2016
Published online 7 APR 2016

On the infrasound detected from the 2013 and 2016 DPRK's underground nuclear tests

J. D. Assink[1], G. Averbuch[2], P. S. M. Smets[1,2], and L. G. Evers[1,2]

[1]R&D Seismology and Acoustics Department, Royal Netherlands Meteorological Institute (KNMI), De Bilt, Netherlands, [2]Department of Geoscience and Engineering, Faculty of Civil Engineering and Geosciences, Delft University of Technology, Delft, Netherlands

Abstract The underground nuclear tests by the Democratic People's Republic of Korea (DPRK) generated atmospheric infrasound both in 2013 and 2016. Clear detections were made in the Russian Federation (I45RU) and Japan (I30JP) in 2013 at stations from the International Monitoring System. Both tropospheric and stratospheric refractions arrived at the stations. In 2016, only a weak return was potentially observed at I45RU. Data analysis and propagation modeling show that the noise level at the stations and the stratospheric circumpolar vortex were different in 2016 compared to 2013. As the seismic magnitude of the 2013 and 2016 nuclear test explosions was comparable, we hypothesize that the 2016 test occurred at least 1.5 times deeper. In such a case, less seismic energy would couple through the lithosphere-atmosphere interface, leading to less observable infrasound. Since explosion depth is difficult to estimate from seismic data alone, this motivates a synergy between seismics and infrasonics.

1. Introduction

Sources of seismic energy in the subsurface can generate low-frequency acoustic waves in the atmosphere, i.e., infrasound. Examples of such sources are earthquakes and explosions [*Donn and Posmentier*, 1964]. There are various mechanisms through which seismic waves in the subsurface can couple to infrasonic waves in the atmosphere at the lithosphere-atmosphere interface. Previous studies with earthquake recordings have shown the following: (1) epicentral infrasound, (2) topographical infrasound, and (3) evanescently coupled infrasound. (1) Epicentral infrasound is the direct coupling of seismic-to-infrasonic energy at the earthquake's epicenter, due to the movement of the Earth's surface [*Mutschlecner and Whitaker*, 2005]. (2) Topographical infrasound can be generated away from the epicentral region by the movement of mountain ranges [*Le Pichon et al.*, 2006] or steep slopes, like a cliff [*Green et al.*, 2009]. Here also, the movement of the Earth's surface due to seismic waves is the source of infrasonic waves [*Walker et al.*, 2013]. (3) Evanescently coupled infrasound has been observed from an earthquake under the ocean. Secondary sources in the water column generated hydroacoustical waves. The ocean-atmosphere interface became anomalously transparent, since the underwater source depths were within one acoustic wavelength, generating infrasound in the atmosphere [*Evers et al.*, 2014].

When a source in the subsurface is capable of generating infrasound, there is no guarantee that the infrasound generated will be detected at a distant station. This strongly depends on the source-receiver distance, the atmospheric winds and temperature, and noise levels at the receiver due to wind and turbulence. In long-range infrasound propagation, i.e., over distances of more than 100 km, the state of the stratosphere [*Assink et al.*, 2014; *Waxler et al.*, 2015] and to a lesser extent the thermosphere determine the (un)favorable conditions for detection.

The Democratic People's Republic of Korea (DPRK) has tested four nuclear devices over the last years (2006, 2009, 2013, and 2016) [*Selby*, 2010; *Wen and Long*, 2010]. All four tests took place at the Punggye-ri Nuclear Test Site in the northeast of the country (see Figure 1). It is a mountainous area, mainly consisting of granite. Details on the source are listed in Table 1 and are derived with seismic stations from the global International Monitoring System (IMS). The IMS is in place for the verification of the Comprehensive Nuclear-Test-Ban Treaty. Next to seismic stations, the IMS also consists of radionuclide, hydroacoustic, and infrasonic measurement devices [*Dahlman et al.*, 2009]. Recordings from the latter will be used in this study. The closest IMS infrasonic stations to the Punggye-ri site are in the Russian Federation (I45RU) and Japan (I30JP), as shown in Figure 1.

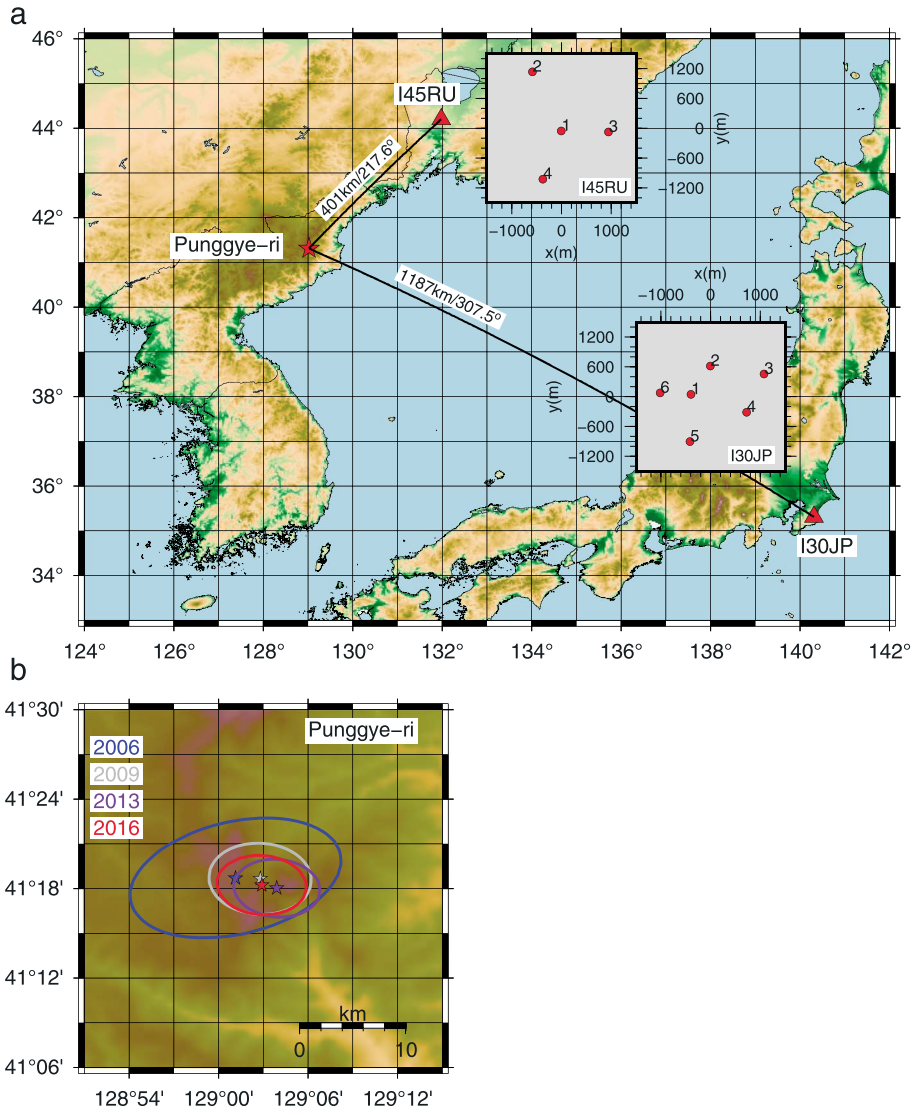

Figure 1. (a) Map showing the DPRK's Punggye-ri Nuclear Test Site in the northeast of the country. The IMS infrasound arrays and their configurations of microbarometers are also shown, being I45RU in the Russian Federation and I30JP in Japan. Element 2 from I45RU was missing in 2013 and element 3 from I30JP in 2016. (b) Map showing the locations of the nuclear test at the Punggye-ri site from 2006, 2009, 2013, and 2016. The uncertainty ellipses are also shown, as derived from IMS seismic recordings (see Table 1 for details).

Table 1. Details From the DPRK's Nuclear Tests Using the IMS

Date[b]	Time (UTC)	Latitude (deg)	Longitude (deg)	Uncertainty (km^2)	m_b	Yield[a] (kt TNT)
2006/10/09	01:35:27.58	41.3119	129.0189	880	4.1	~1
2009/05/25	00:54:42.80	41.3110	129.0464	265	4.5	~5
2013/02/12	02:57:50.80	41.3005	129.0652	181	4.9	~10
2016/01/06	01:30:00.49	41.3039	129.0481	193	4.8	<10

[a]Yield estimates were obtained from NORSAR, as published at http://www.norsar.no/norsar/about-us/News/North-Korea-nuclear-test-on-6-January-2016, last accessed 2016.01.21.
[b]Dates are formatted as year/month/day.

Infrasound has not been detected on IMS infrasound stations from the 2006 and 2009 tests. Non-IMS infrasound stations will not be considered here [*Che et al.*, 2009]. A suggested fifth test in 2010 is disputed and will not be discussed, as it would have had a too small yield to be detected with infrasound [*Zhang and Wen*, 2015].

In this study, it is discussed why infrasound from the 2013 DPRK nuclear test was clearly detected and why the 2016 test left a less clear signature in the atmosphere. Although the source strengths were comparable, the source depth, the state of the upper atmosphere, and receiver noise levels appear to have played an important role in the detectability of infrasound. Since the depth of an explosion is difficult to estimate from seismic data alone [*Bowers and Selby*, 2009], this motivates a synergy between the seismic and infrasound technologies to improve on the depth estimation of (nuclear) explosions.

2. Atmospheric Propagation of Infrasound in 2013 and 2016

Infrasound can travel over long ranges, because of its low-frequency contents and since several waveguides exist in the atmosphere, in which acoustic energy can be trapped. Three waveguides between the Earth's surface and upper atmosphere exist: (1) The tropospheric waveguide with its upper bound in the tropopause (~10 km), caused by the jet stream; winds at a lower level and temperature inversions can also form a tropospheric waveguide; (2) the stratospheric waveguide with its upper limit around the stratopause (~50 km), formed by the temperature increase due to the presence of ozone and the circumpolar vortex; and (3) the thermospheric waveguide from the mesopause (~90 km) and upward, due to the increase in temperature. However, infrasonic waves are much attenuated at these altitudes in the highly rarefied atmosphere.

The wind strength and direction, as a function of altitude, make the atmosphere a highly anisotropic medium for the propagation of infrasound. Typically, infrasound is detected in the downwind direction. The westerly jet stream near the tropopause directs the infrasound to the east, while the direction of circumpolar vortex changes direction between the equinoxes. On the Northern Hemisphere, the polar vortex is directed to the east in winter and west in summer. The summer stratosphere is stable, but in winter planetary waves from the troposphere can propagate into the stratosphere. Interaction of such waves with the polar vortex can lead to sudden stratospheric warmings (SSWs). Even bidirectional waveguides can be formed under such circumstances [*Assink et al.*, 2014]. These SSWs occur every winter and can be minor or major. In the latter case, stratospheric winds reverse and the temperature increases with tens of degrees Celsius in only a few days. These conditions strongly affect infrasound propagation [*Evers and Siegmund*, 2009; *Evers et al.*, 2012; *Smets and Evers*, 2014].

Infrasonic propagation can be modeled in a high-frequency approach by applying ray tracing. However, such an approach does not cover full wave effects like scattering and diffraction. Therefore, other methods, such as the parabolic equation method, are used, which account for full wave phenomena [*Collins*, 1993]. Inputs necessary for the propagation modeling are atmospheric specifications of density, temperature, and wind. Especially, the latter two are highly variable as a function of altitude, time, and geographical location. The European Centre for Medium-Range Weather Forecasts (ECMWF) provides hourly global atmospheric specifications with a spatial resolution of 0.125°, up to 0.01 hPa (~79 km altitude).

Figure 2 shows the ECMWF's wind and temperature specifications near the stratopause (1.5 hPa or ~45 km). In February 2013, there was a well-developed circumpolar vortex around the cold Arctic stratosphere. In contrast, in January 2016, the vortex was displaced from its circumpolar trajectory and a warm stratosphere was present over the area of interest. The eastward vortex, as in 2013, is no longer present, and a mixture of eastward and westward wind directions is visible over the area of interest. Such a state of the stratosphere is formed in the early stages of a SSW. The results on the propagation of these different wind and temperature conditions, between the years, are shown in Figure 3.

Well-formed tropospheric and stratospheric waveguides are present for I45RU in 2013. Both waveguides exist due the strong winds near the tropopause and stratopause. Comparing the adiabatic and effective sound speeds, which takes into account the wind effect, shows that the jet stream and circumpolar vortex, respectively, lead to a downward refracting atmosphere. In 2016, tropospheric and weak stratospheric refractions are predicted to reach I45RU. The stratospheric paths interact with the troposphere but have a relatively large transmission loss, due to the weaker vortex. Tropospheric refractions are predicted for I30JP in both 2013 and 2016, which are caused by the jet stream. A weak stratospheric return might be observed in 2013. However, the partly counteracting circumpolar vortex in 2016 will prevent such a stratospheric refraction. In 2016, the

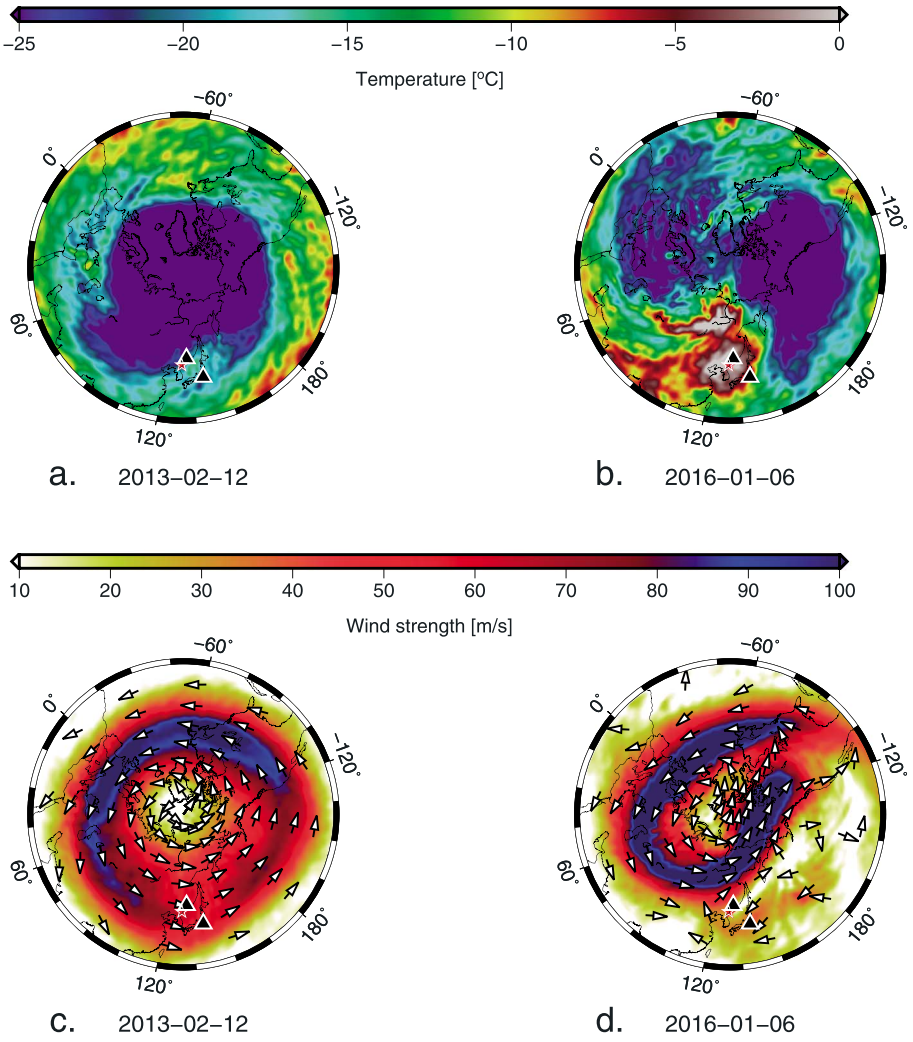

Figure 2. The wind and temperature at 1.5 hPa (~45 km) from ECMWF atmospheric specifications. IMS infrasound stations are indicated with the black triangles, being I45RU to the north of Punggye-ri (star) and I30JP to the east. The temperatures are given in (a) 2013/02/12 03:00 UTC and (b) 2016/01/06 02:00 UTC. The wind strength and direction are shown in (c) 2013 and (d) 2016.

refraction altitude is higher than that in 2013, which leads to a stronger attenuation. Furthermore, the strong jet stream hardly allows refractions to reach the Earth's surface. A so-called elevated waveguide has formed. The transmission losses at each array are given in Table 2.

3. Infrasound Detections of the 2013 and 2016 Tests

Infrasound is measured with arrays of microbarometers (see Figure 1), which are sensitive in the frequency range of at least 0.02 to 4 Hz. Within this range, small-sized atmospheric nuclear tests of about 1 kt trinitrotoluene (TNT) can be detected, as these are expected to generate infrasound of 0.1 to 0.2 Hz. Underground tests can generate higher frequencies in the atmosphere, as the seismic wavefield contains more higher frequencies. The advantage of measuring with arrays is twofold. (1) The noise due to wind and turbulence is reduced by summing the signals of the individual microbarometers. Those are spaced at such a distance that the wind field leaves an incoherent pressure field, while the long wave lengths of the infrasound are coherent. (2) The apparent velocity of the infrasonic wave can be estimated, being a measure of the angle of incidence of the wave. Furthermore, the direction of arrival or back azimuth can be obtained. In order to do so, beamforming is applied to the individual recordings, by time delaying and summing the recordings.

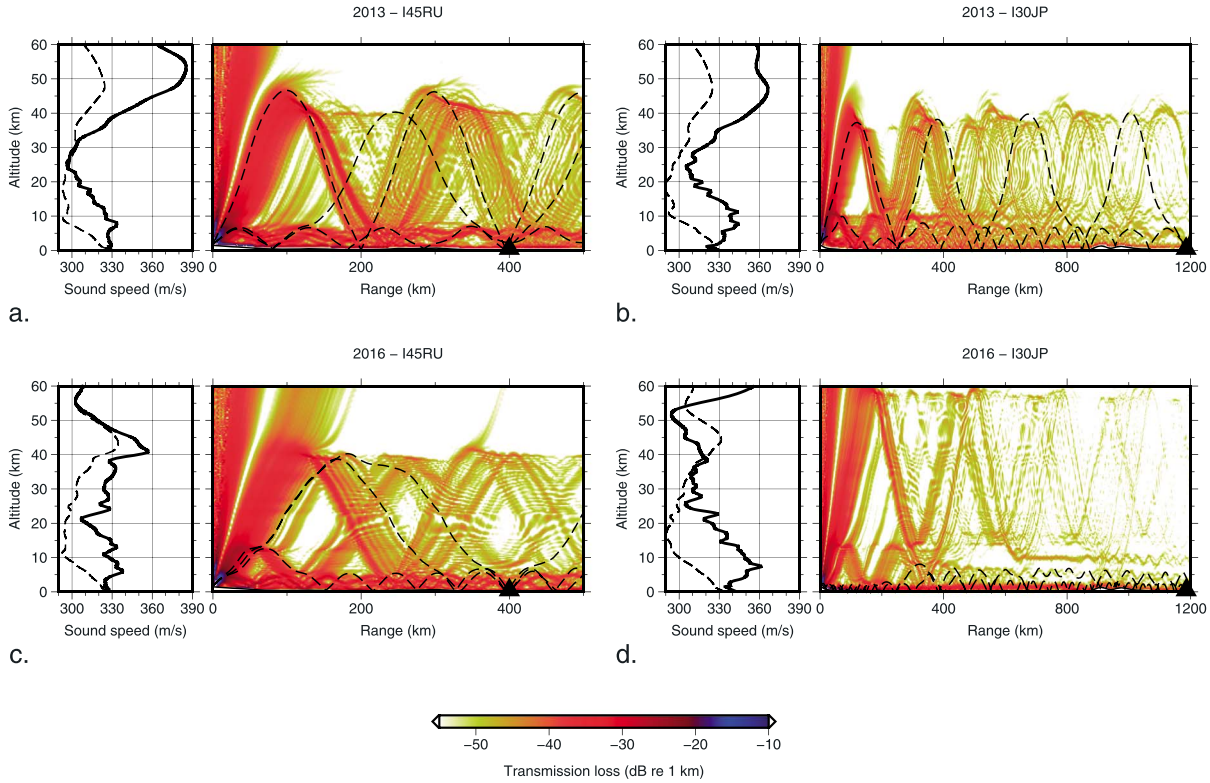

Figure 3. The propagation of infrasound from the Punggye-ri Nuclear Test Site to the IMS infrasound stations, for I45RU in (a) 2013 and (c) 2016 and for I30JP in (b) 2013 and (d) 2016. The transmission loss is shown as a function of distance and altitude at 1.0 Hz. The eigenrays that connect the source and receiver are shown as dashed lines. The adiabatic (dashed line) and effective sound speeds (solid line) are given in separate frames, to the left of each propagation frame. These profiles are taken at the midpoint between source and receiver. In Table 2 the exact transmission loss values are given.

Continuous infrasonic recordings are processed based on the signal coherency, with a sliding window approach. An increase in signal coherency over the array indicates the presence of an infrasonic wave. The Fisher ratio is a sensitive measure of the signal coherency or signal-to-noise ratio (SNR) [*Melton and Bailey*, 1957].

Array processing results are shown for the I45RU and I30JP infrasonic recordings in 2013 and 2016 in Figure 4. I45RU clearly detects both tropospheric (I_w) and stratospheric (I_s) refractions in 2013. An intermediate return (I_{ws}) is also identified, which is a signal that has leaked from the troposphere to the stratosphere (see also Figure 3). The expected arrival time, back azimuth, and apparent velocity (blue dots) from ray tracing and the observations (red dots) are in agreement. The increase in apparent velocity as a function of time is representative for the increase in refractions altitude. Furthermore, the celerities (horizontal distance divided by traveltime), as given in the SNR frame, correspond to the expected values for tropospheric and stratospheric returns [*Brown et al.*, 2002]. Other local impulsive sources with a high SNR are visible throughout the recording.

Table 2. Transmission Loss in dB Referenced to 1 km at 1.0 Hz, for Tropospheric (I_w) and Stratospheric (I_s) Refractions

	I_w	I_s
	2013	
I45RU	−37.7	−47.9
I30JP	−53.4	−53.4
	2016	
I45RU	−38.1	−53.0
I30JP	−50.6	−67.5

In 2016, only one arrival is potentially identified at I45RU. This arrival can be associated with the tropospheric and both stratospheric propagation paths (Figure 3c), considering the observations and the modeled parameters. The detection is very weak, and its identification is much dependent on the processing parameters. In that sense, it is a rather unstable detection that might be missed with different settings for the bin size, overlap, and corner frequencies of the band-pass

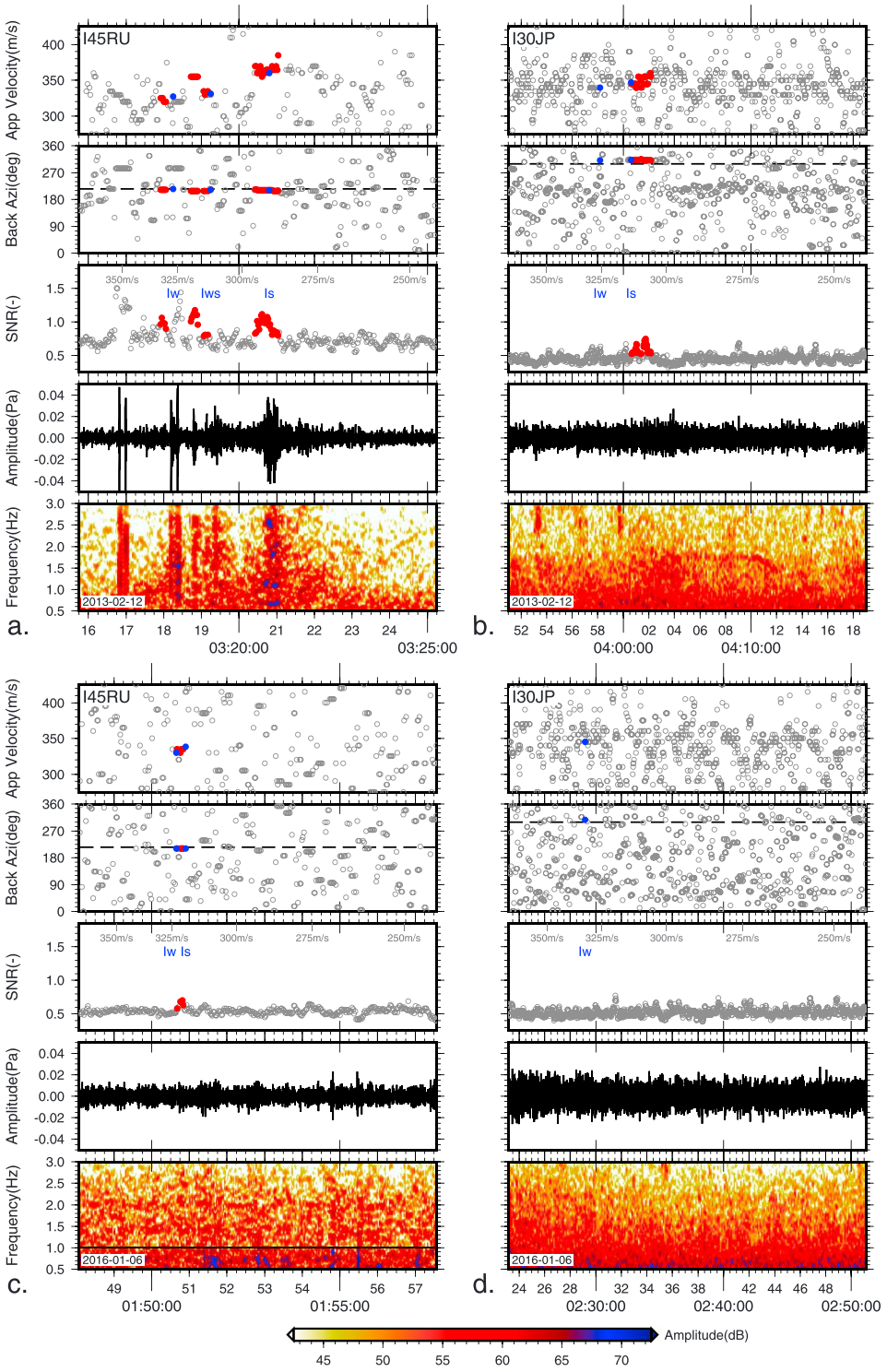

Figure 4. Results from array processing the infrasonic recording of I45RU in (a) 2013 and (c) 2016 and those for I30JP in (b) 2013 and (d) 2016. For each array and date, a set of four frames is shown to characterize the signals. Shown are subsequently the spectral contents, the best beam, the signals-to-noise ratio (SNR), the back azimuth (with the true back azimuth as dashed line), and the apparent velocity, from bottom to top and as a function of time. The celerities are given in m/s in the SNR frame. The red dots indicate events of interest which are also labeled as I_w, I_{ws}, and I_s for, respectively, tropospheric, combined tropospheric-stratospheric, and stratospheric refractions. The blue dots follow from three-dimensional ray tracing (in spherical coordinates) through ECMWF atmospheric specifications. The following settings were used to obtain these results: bin size 256 samples, overlap 224 samples, second-order Butterworth filter with two passes, and corner frequencies of 0.5 to 3.0 Hz (for I45RU 2016 1.0 to 3.0 Hz).

filter. The local noise levels in 2016 are higher than those in 2013, as can be seen from the high spectral values in the spectrograms, outside the times signal is present. ECMWF surface winds are 2.4 m/s in 2016 and 0.9 m/s in 2013, which are consistent with higher noise levels.

Tropospheric returns are not observed in I30JP neither in 2013 nor in 2016. The only refractions that could be identified is a stratospheric return in 2013. Noise levels from the spectral amplitudes seem not to differ too much. The surface winds in 2016 are only slightly higher than those in 2013, i.e., 1.9 versus 1.6 m/s.

4. Discussion and Conclusions

The underground nuclear tests conducted by the DPRK in 2013 and 2016 both generated observable atmospheric infrasound. Clear signatures were obtained in the Russian Federation by IMS array I45RU and in Japan by I30JP in 2013. At I45RU both tropospheric and stratospheric refractions were identified from the 2013 test. In 2016, only a weak return could potentially be found at I45RU. The stratospheric refraction detected at I30JP in 2013 was not observed in 2016.

The following explanations are postulated based on observations and modeling.

1. The 2016 stratosphere was disturbed by planetary waves interacting with the circumpolar vortex, i.e., a possible early stage SSW. Propagation of infrasound through the stratosphere was unfavorable for I30JP. This also follows from the transmission loss modeling (see Table 2).
2. The local noise levels at I45RU due to wind were higher in 2016 than in 2013, which can obscure a clear detection.
3. It should be noted that the detection capability of I45RU was higher in 2016 than in 2013, since one of the microbarometers (element 2) was missing in 2013.
4. The size of the nuclear test, in terms of yield, might be somewhat smaller in 2016 (m_b 4.8) than in 2013 (m_b 4.9), based on IMS magnitudes. Therefore, less energy was possibly coupled into the atmosphere. However, it should be noted that this difference in magnitudes falls within the typical range of uncertainties. Indeed, comparable seismic moment magnitudes have been estimated for the 2013 (M_w = 4.7) and 2016 (M_w = 4.71) events [*Incorporated Research Institutions for Seismology (IRIS)*, 2013, 2016], as well.

It should be noted that we have not considered scattering off small-scale structure, such as caused by subgrid-scale gravity waves [e.g., *Kulichkov et al.*, 2010], which could likely further enhance the stratospheric propagation efficiency, in particular for the 2016 case.

The lack of detections of tropospheric refractions at I30JP can only be explained by the fact that the waveguide is very thin and its continuity can be disrupted by wind and turbulence.

The fact that (1) tropospheric propagation toward I45RU was similar in 2013 and 2016 and no clear tropospheric detection could be made at I45RU in 2016, (2) no clear stratospheric returns were identified at I45RU in 2016, though possible from the transmission loss calculations, and (3) the seismic magnitudes of the 2013 and 2016 test explosions were comparable and motivate us to hypothesize that the 2016 test was at a greater depth than the 2013 test.

Based on a preliminary analysis of relative source depths of the 2013 and 2016 explosions (Text S1), we estimate that the 2016 test took place at least 1.5 times deeper than the 2013 test. Assuming a minimum source depth of 450 m for the 2013 test, based on hydrodynamic simulation results [*Rougier et al.*, 2011] and the 2013 yield estimate of 10 kt TNT (Table 1), this would imply that the 2016 explosion would have occurred at least 225 m deeper.

Such an explanation could indeed explain the reduced coupling of seismic energy through the lithosphere-atmosphere interface. However, this hypothesis should be further tested to investigate the effects of differences in rock conditions as well as uncertainties in yield estimates and atmospheric structure.

Future studies, involving a more extensive observational data set and numerical modeling that accounts for lithosphere-atmosphere coupling and varying geological conditions, will be conducted to further test this hypothesis and to provide quantitative constraints on the source depth.

As the depth of an explosion is difficult to estimate from seismic data alone [*Bowers and Selby*, 2009], infrasound may thus provide useful complementary information.

Acknowledgments
The authors thank the CTBTO and station operators for the high quality of IMS data and products. IMS data can be accessed through the vDec (see https://www.ctbto.org/specials/vdec/). All figures have been created using Generic Mapping Tools [*Wessel et al.*, 2013]. ECMWF atmospheric specifications are available to Member States. G.A. is funded through the Marie Curie Action WAVES from the European Union within H2020, grant 641943. P.S. is funded through the ARISE2 project from the European Union within H2020, project 653980. L.E.'s contribution is partly funded through a VIDI project from the Dutch Science Foundation (NWO), project 864.14.005. The authors are grateful for helpful reviews by the Editor and two anonymous reviewers.

References

Assink, J. D., R. Waxler, P. Smets, and L. G. Evers (2014), Bidirectional infrasonic ducts associated with sudden stratospheric warming events, *J. Geophys. Res. Atmos.*, *119*, 1140–1153, doi:10.1002/2013JD021062.

Bowers, D., and N. D. Selby (2009), Forensic seismology and the comprehensive nuclear-test-ban treaty, *Annu. Rev. Earth Planet. Sci.*, *37*, 209–236, doi:10.1146/annurev.earth.36.031207.124143.

Brown, D. J., C. N. Katz, R. Le Bras, M. P. Flanagan, J. Wang, and A. K. Gault (2002), Infrasonic signal detection and source location at the prototype international data centre, *Pure Appl. Geophys.*, *159*(5), 1081–1125, doi:10.1007/s00024-002-8674-2.

Che, I.-Y., T. S. Kim, J.-S. Jeon, and H.-I. Lee (2009), Infrasound observation of the apparent North Korean nuclear test of 25 May 2009, *Geophys. Res. Lett.*, *36*, L22802, doi:10.1029/2009GL041017.

Collins, M. D. (1993), A split-step Padé solution for the parabolic equation method, *J. Acoust. Soc. Am.*, *93*(4), 1736–1742, doi:10.1121/1.406739.

Dahlman, O., P. Mykkeltveit, and H. Haak (2009), Monitoring technologies, in *Nuclear Test Ban*, chap. 2, pp. 1–34, Springer, Dordrecht, doi:10.1007/978-1-4020-6885-0_2.

Donn, W. L., and E. S. Posmentier (1964), Ground-coupled air waves from the Great Alaskan Earthquake, *J. Geophys. Res.*, *69*(24), 5357–5361, doi:10.1029/JZ069i024p05357.

Evers, L. G., and P. Siegmund (2009), Infrasonic signature of the 2009 major sudden stratospheric warming, *Geophys. Res. Lett.*, *36*, L23808, doi:10.1029/2009GL041323.

Evers, L. G., A. R. J. van Geyt, P. Smets, and J. T. Fricke (2012), Anomalous infrasound propagation in a hot stratosphere and the existence of extremely small shadow zones, *J. Geophys. Res. Atmos.*, *117*, D06120, doi:10.1029/2011JD017014.

Evers, L. G., D. Brown, K. D. Heaney, J. D. Assink, P. S. M. Smets, and M. Snellen (2014), Evanescent wave coupling in a geophysical system: Airborne acoustic signals from the M_W 8.1 Macquarie Ridge earthquake, *Geophys. Res. Lett.*, *41*, 1644–1650, doi:10.1002/2013GL058801.

Green, D. N., J. Guilbert, A. Le Pichon, O. Sebe, and D. Bowers (2009), Modelling ground-to-air coupling for the shallow ML 4.3 folkestone, United Kingdom, earthquake of 28 April 2007, *Bull. Seismol. Soc. Am.*, *99*(4), 2541–2551, doi:10.1785/0120080236.

Incorporated Research Institutions for Seismology (IRIS) (2013), Special Event: North Korea nuclear explosion, Washington, D. C. [Available at http://ds.iris.edu/ds/nodes/dmc/specialevents/2013/02/12/ north-korea-nuclear-explosion/, accessed 16 March 2016.]

Incorporated Research Institutions for Seismology (IRIS) (2016), Special Event: 2016 North Korean nuclear test, Washington, D. C. [Available at https://ds.iris.edu/ds/nodes/dmc/specialevents/2016/01/05/2016-north-korean-nuclear-test/, accessed 16 March 2016.]

Kulichkov, S. N., I. P. Chunchuzov, and O. I. Popov (2010), Simulating the influence of an atmospheric fine inhomogeneous structure on long-range propagation of pulsed acoustic signals, *Izv. Atmos. Ocean. Phys.*, *46*, 60–68.

Le Pichon, A., P. Mialle, J. Guilbert, and J. Vergoz (2006), Multistation infrasonic observations of the Chilean earthquake of 2005 June 13, *Geophys. J. Int.*, *167*(2), 838–844, doi:10.1111/j.1365-246x.2006.03190.x.

Melton, B., and L. Bailey (1957), Multiple signal correlators, *Geophysics*, *22*(3), 565–588, doi:10.1190/1.1438390.

Mutschlecner, J. P., and R. W. Whitaker (2005), Infrasound from earthquakes, *J. Geophys. Res.*, *110*, D01108, doi:10.1029/2004JD005067.

Rougier, E., H. J. Patton, E. E. Knight, and C. R. Bradley (2011), Constraints on burial depth and yield of the 25 May 2009 North Korean test from hydrodynamic simulations in a granite medium, *Geophys. Res. Lett.*, *38*, L16316, doi:10.1029/2011GL048269.

Selby, N. D. (2010), Relative locations of the October 2006 and May 2009 DPRK announced nuclear tests using international monitoring system seismometer arrays, *Bull. Seismol. Soc. Am.*, *100*(4), 1779–1784, doi:10.1785/0120100006.

Smets, P. S. M., and L. G. Evers (2014), The life cycle of a sudden stratospheric warming from infrasonic ambient noise observations, *J. Geophys. Res. Atmos.*, *119*(21), 12,084–12,099, doi:10.1002/2014JD021905.

Walker, K. T., A. L. Pichon, T. S. Kim, C. de Groot-Hedlin, I.-Y. Che, and M. Garcés (2013), An analysis of ground shaking and transmission loss from infrasound generated by the 2011 Tohoku earthquake, *J. Geophys. Res. Atmos.*, *118*(23), 12,831–12,851, doi:10.1002/2013JD020187.

Waxler, R., L. G. Evers, J. D. Assink, and P. Blom (2015), The stratospheric arrival pair in infrasound propagation, *J. Acoust. Soc. Am.*, *137*(4), 1846–1856, doi:10.1121/1.4916718.

Wen, L., and H. Long (2010), High-precision location of North Korea's 2009 nuclear test, *Seismol. Res. Lett.*, *81*(1), 26–29.

Wessel, P., W. H. F. Smith, R. Scharroo, J. Luis, and F. Wobbe (2013), Generic mapping tools: Improved version released, *Eos Trans. AGU*, *94*(45), 409–410, doi:10.1002/2013EO450001.

Zhang, M., and L. Wen (2015), Seismological evidence for a low-yield nuclear test on 12 May 2010 in North Korea, *Seismol. Res. Lett.*, *86*(1), 138–145, doi:10.1785/02201401170.